Marine Structures 84 (2022) 103230

Contents lists available at ScienceDirect

Marine Structures

journal homepage: www.elsevier.com/locate/marstruc

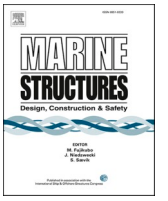

Numerical study on buckling of aluminum extruded panels considering welding effects

Xintong Wang [a,*], Jørgen Amdahl [a], Olav Egeland [b]

[a] Centre for Autonomous Marine Operations and Systems, Department of Marine Technology, Norwegian University of Science and Technology, Trondheim, 7491, Norway
[b] Department of Mechanical and Industrial Engineering, Norwegian University of Science and Technology, Trondheim, 7043, Norway

ARTICLE INFO

Keywords:
Numerical simulation
Aluminum extruded panels
Buckling
Welding effects

ABSTRACT

Aluminum extruded panels are increasingly used in marine structures as lightweight solutions. Less welding is needed for such extrusions than traditional built-up panels of welding stiffener to plate sheets. However, the buckling mode and ultimate strength of aluminum extruded panels are difficult to predict with existing formulas due to different welding sensitivity. This paper presents a numerical study on the buckling of aluminum extruded panels, with the effects of welding taken into account. The numerical study was done with the nonlinear finite element method. The simulations were verified by comparing them with experimental results from the literature. The sensitivity of the ultimate load with respect to the welding effects was determined by parametric studies. The effect of inertia forces on the stiffener-tripping buckling mode was investigated. The influence of the slenderness ratio on the heat-affected zone (HAZ) effects was analyzed. The simulations can be also used as a foundation for developing improved analytical formulations.

1. Introduction

The lightweight design of stiffened panels can increase the energy efficiency of marine structures. With a high strength-to-weight ratio, aluminum alloys are useful solutions for reducing weight while maintaining strength [1]. Currently, aluminum alloys are increasingly being used in marine structures such as high-speed vessels, helicopter decks, gangways, and living quarters [2]. However, there are also challenges in the use of aluminum alloys. Aluminum alloys behave differently than steel after yielding. The temperature-dependent softening of aluminum makes aluminum sensitive to welding. Furthermore, it is difficult to obtain data on the imperfections caused by the manufacturing process. Thus, the existing ultimate strength-based design methods commonly used for steel structures cannot be directly applied to aluminum structures.

Several investigations on the ultimate strength of aluminum marine structures have been conducted to develop a better design method. The buckling strength of aluminum-stiffened panels under axial or transverse compression has been tested experimentally [3–8]. Although relatively few experiments have been conducted due to the associated costs, realistic information about material properties, initial imperfections and ultimate strength could still be obtained from existing tests. Numerical simulations, such as the finite element method, have been commonly used [5–15]. In addition to investigations of the ultimate strength of unstiffened and stiffened plates, larger structures, such as ship hull girders, have been simulated. Parametric analyses of geometries, imperfections, heat affect zones (HAZ), boundary conditions, and load combinations have been performed [12,14–17]. Some analytical ultimate

* Corresponding author.
E-mail address: xintong.wang@ntnu.no (X. Wang).

https://doi.org/10.1016/j.marstruc.2022.103230
Received 13 December 2021; Received in revised form 4 March 2022; Accepted 1 April 2022
Available online 18 April 2022

strength formulations have also been developed based on the steel structural design method, energy method or empirical method from the database of experiments/simulations in the literature [18–20]. For a more detailed review of the research on the ultimate strength of aluminum marine structures, please refer to the work by Hosseinabadi and Khedmati [21].

Although the ultimate strength of aluminum-stiffened panels fabricated by conventional welding have been extensively studied, research focusing on aluminum extruded panels is limited. Because less welding is needed to construct aluminum marine structures with extruded panels, fewer welding-induced geometrical and mechanical imperfections are introduced into the structure, potentially improving the ultimate strength. This advantage over traditional welded aluminum panels has led to an increasing interest in extruded panels. However, the buckling mode and ultimate strength of aluminum extruded panels are difficult to predict with existing design formulations. Therefore, numerical simulations are necessary.

In the present work, buckling of aluminum extruded panels were investigated by the nonlinear finite element method, with the effects of welding taken into account. The numerical simulations were verified by comparing them to a series of uniaxial compression experiments by Aalberg et al. [3], which are denoted as 'reference experiments' in the following discussions. In the reference experiments, extruded panels either with one open (L-shaped) or one closed stiffener were made of AA6082-T6 alloys. Metal inert gas (MIG) welding and friction stir welding (FSW) were used to butt weld larger panels with open and closed stiffeners, respectively. The initial imperfections were measured in the center of each extruded panel. The engineering stress-strain curves of the plate material, stiffener material and HAZ material were obtained via uniaxial coupon tensile tests. The panels were arranged vertically in the test rig, as shown in Fig. 1. Steel bearings were used at both the upper and lower ends to apply the load. The upper end was loaded with an axial compressive displacement via a stiff loading beam, while the reaction force was obtained at the lower end. Simply supported or free boundary conditions were designed for the unloaded ends.

The remainder of this paper is structured as follows: The setup for the numerical simulations is discussed in Section 2. The load end-shortening curves and the ultimate strength obtained in the simulations and the tests are compared in Section 3. The influence of the inertia force and HAZ content on the ultimate strength is discussed. The conclusions are presented in Section 4.

2. Simulation setups

2.1. Panel geometries

The aluminum-stiffened panels in the reference experiments were welded from extruded panels. The geometries of two typical profiles are shown in Fig. 2. The dimensions of the various cases are given in the appendix. The geometry of the welded panels varied, with lengths of 1 m or 2 m and widths of three or five extruded panels.

In the simulations, shell elements were built along the centerlines of the profile cross-sections with realistic dimensions. Then, the panels were assembled and merged by three or five identical profiles.

2.2. Material model

The Ramberg-Osgood relationship has been widely adopted due to its ability to simulate the behavior of aluminum during finite strains. The strain-stress relationship is given as:

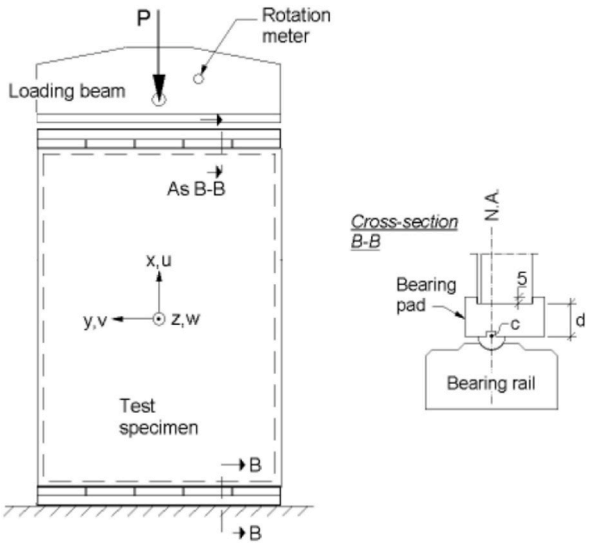

Fig. 1. Test setup and cross-section of cylindrical thrust bearings at the loaded ends in the reference experiments [3].

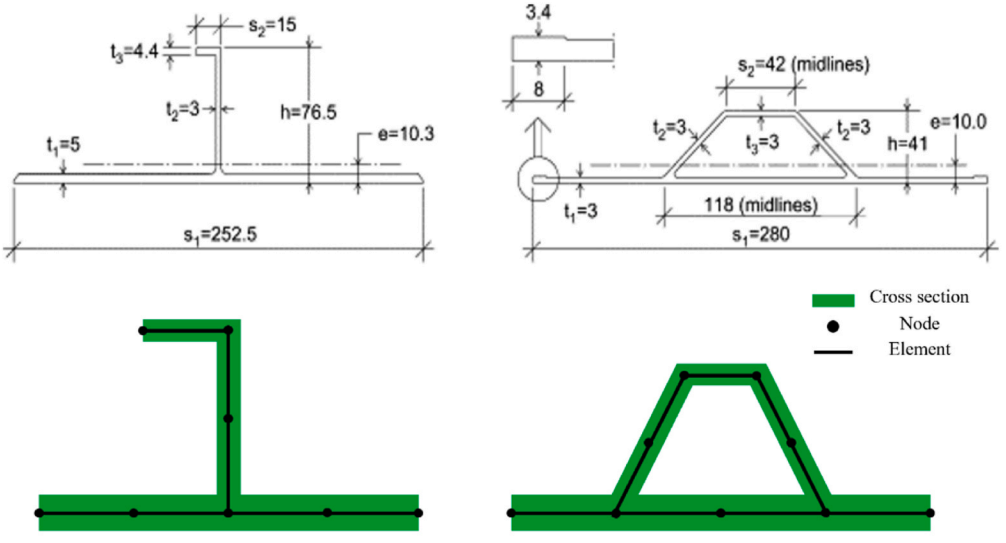

Fig. 2. Cross-sectional geometry of extruded panels in reference experiments (above) [3] and numerical simulations (below). The mesh is shown approximately.

$$\varepsilon = \frac{\sigma}{E} + 0.002\left(\frac{\sigma}{\sigma_y}\right)^n \tag{2.1}$$

where.

ε is the strain,

σ is the stress.

E is the Young's modulus,

σ_y is the yield stress at the 0.2% offset strain, called the proof stress,

and n is a constant that depends on the material being considered. A large n indicates a small strain-hardening feature.

The parameters in the Ramberg-Osgood relationship were determined based on the reference experiments. The Young's modulus was calibrated according to the stress-strain curves from the tensile tests. The constant n was determined by the ultimate point and the yield point. The former was obtained from the stress-strain curves, while the latter was represented by the mean proof stress, f_{02}. Though the mean proof stress of HAZ materials was not directly specified for each case in the reference experiments, a range of 50%–60% of that of the parent plate material was reported in example tests. Thus, a high value of 60% was assumed considering that the proof yield stresses in the HAZ are uneven and hardening areas always exist as observed by Rønning et al. [4]. The material parameters used in the simulations are listed in Table 1.

The material model was assigned via the ABAQUS built-in Ramberg-Osgood material 'Deformation Plasticity'. The stress-strain curves used in the simulations are shown in Fig. 3, where the materials of Panel A were taken as examples.

2.3. Welding effects

The welding effects induced by the heat input include mechanical (material softening and residual stress) and geometrical (initial deformations) imperfections [8]. Both effects were modelled in the simulations, as shown in Fig. 4. Panel A, which had with closed stiffeners, and Panel H, which had L-shaped stiffeners, were taken as examples. The measured distortion levels are also provided in Fig. 4.

Table 1
Adopted material parameters of the Ramberg-Osgood model in simulations [3].

Panel No.	Plate		Stiffener		HAZ	
	σ_y [MPa]	n [−]	σ_y [MPa]	n [−]	σ_y [MPa]	n [−]
A	286	35.6	277	23.6	171.6	12
B, C, D E, F, G, P, Q	261	18.3	275	22.4	156.6	9.12
H	309	179	302	58.8	185.4	16.3
I	255	16.3	265	18	153	8.61
J, K, R, S	254	16	270	20	152.4	8.51
L, M, T, U	265	19.9	284	28.5	159	9.49
N, O	265	19.9	275	22.4	159	9.49

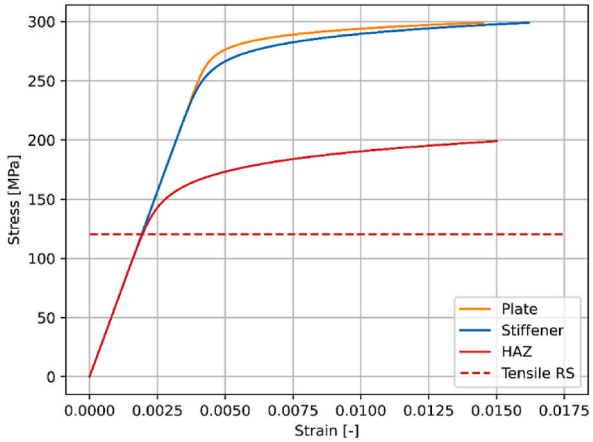

Fig. 3. True stress-strain curves of assigned materials in simulations. The value of the introduced tensile residual stress is displayed as a dashed line.

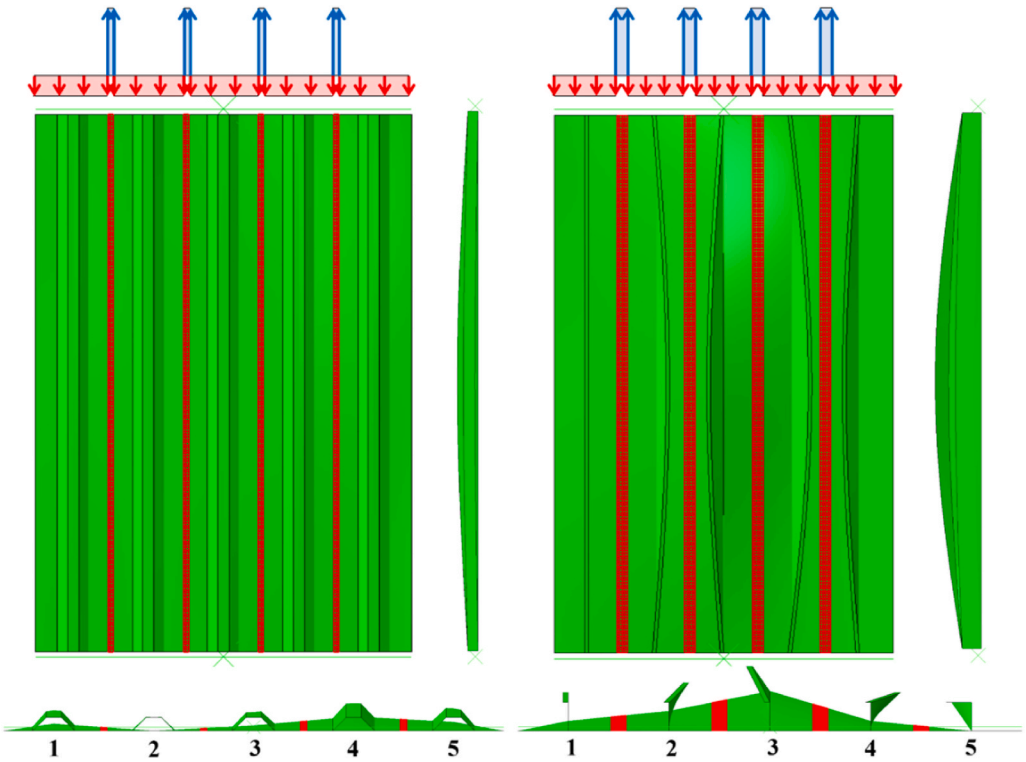

Panel A	1	2	3	4	5
Vertical deflection [mm]	+0.4	0.0	+0.3	+0.8	+0.5
Sideway distortion [mm]	-	-	-	-	-

Panel H	1	2	3	4	5
Vertical deflection [mm]	+0.5	+1.0	+2.0	+0.5	0.0
Sideway distortion [mm]	0.0	+1.0	-1.0	+1.5	-1.0

Fig. 4. Schematic illustration of introduced welding effects. The HAZ is displayed in red. The tensile and compressive residual stresses are shown with blue and red arrows, respectively. Imperfections are taken from measurements by Aalberg et al. [3], and are displayed with a magnification factor of 100.

The heat-affected zone (HAZ) was assumed to be 20 mm for MIG welding and 10 mm for FSW on each side, in accordance with the measurements by Rønning et al. [4]. The softened material and tensile residual stress were assumed to be present in the HAZ, while the base material and compressive residual stress were applied outside the HAZ. Only the residual stress components along the welding direction were considered. A tensile residual stress of 70% HAZ material yield stress was assigned through the predefined stress field. The compressive residual stress is calculated as:

$$\sigma_{RS,compression} = \frac{A_{HAZ}}{A_{plate} - A_{HAZ}} \sigma_{RS,tension} \tag{2.2}$$

where.

$\sigma_{RS,compression}$ is the compressive residual stress,

$\sigma_{RS,tension}$ is the tensile residual stress.

A_{HAZ} is the HAZ section area,

and A_{plate} is the section area of the whole plate.

The initial imperfection was applied by moving the nodes. The displacement field was assumed based on the measured vertical deflection of the plates and sideways distortion of the stiffeners at mid span. It was assumed that the imperfection varied smoothly between the measured points and converged to zero at the ends. A single half-sinusoidal wave was assumed in the longitudinal direction of the plates and stiffeners. Linear extrapolation was used in the transverse direction of the plates and the vertical direction of the stiffeners.

2.4. Constraints and boundary conditions

Steel bearing arrangements were used at both ends along the loading direction in the reference experiments to ensure the load transferred exactly in the neutral axis (N.A). A stiff loading beam was used to apply axial compressive displacement, while the reaction force was obtained at the other end. The unloaded edges were either simply supported or free, and transverse in-plane deformations were allowed.

The bearing system of the loaded sides was modelled with rigid beam and multipoint constraints (MPCs), as shown in Fig. 5. The height h and the distance to the cross-section d of the beam center were assigned based on realistic arrangements. The cross-section of the two ends could rotate freely along the beam while restraining any deformations. Simply supported or free boundary conditions were assigned to the longitudinal edges as in the reference experiments.

2.5. Other setups

In the simulations, the 'S4R' element was used. It is a four-node element with reduced integration, hourglass control, and finite membrane strains that is widely used in determining ultimate strength. The 'Dynamic/Implicit, Quasi-static' solver in the ABAQUS software was used to conduct displacement-controlled buckling simulations. The rigid beam moved with a speed of 1.0 mm per minute, as in the reference experiments. The translation distance was adjusted to the maximum axial movement, which was extracted from the reported force end-shortening curves approximately, for each case. The maximum and minimum time increment in the dynamic solver is 1 s and 0.0001 s, respectively. The predefined data would be output every ten increments in ABAQUS.

The mesh size was determined by convergence tests. Four panels are taken as example, as shown in Fig. 6. All reported stiffener profiles and buckling modes were included. It should be noted that the mesh size varied from 10 mm to 2.5 mm for panels with closed stiffeners and from 20 mm to 5 mm for panels with open stiffeners, due to the different HAZ width assumptions. The load end-shortening curve changes very little as the mesh size decreases. Thus, a mesh size of 10 mm was chosen, which balanced the need for accuracy with acceptable computational costs.

The meshed panels are shown in Fig. 7. For panels with L-shaped stiffeners, there are four elements along the HAZ width, seven elements along the web height, and one element along the flange width. For panels with closed stiffeners, there are two elements along the HAZ width, five elements along the web height, and four elements along the flange width. The chosen mesh size was small enough to capture different buckling modes.

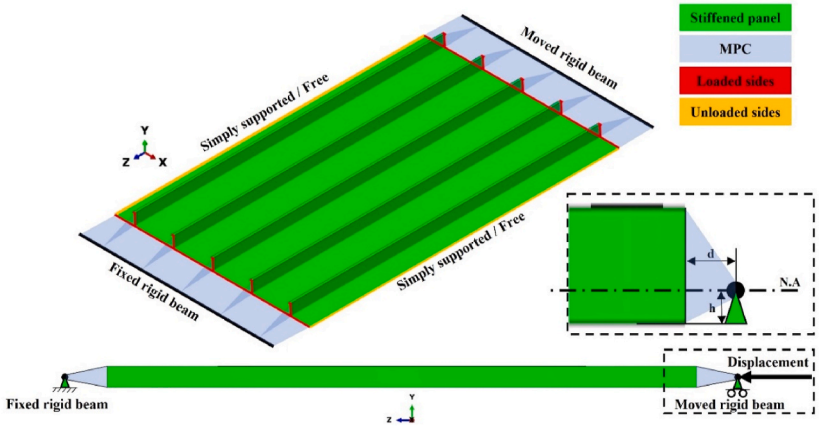

Fig. 5. Schematic illustration of constraints and boundary conditions in simulations.

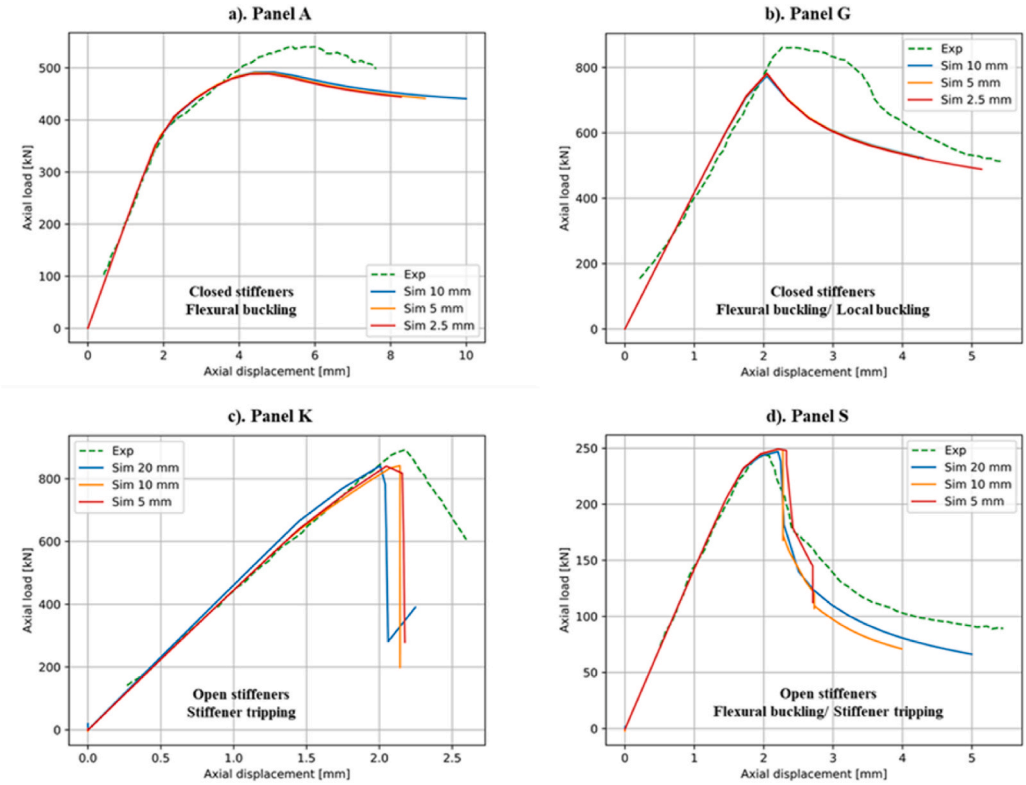

Fig. 6. Load end-shortening curves of convergence tests. 'Exp' indicates the experiments. 'Sim' indicates the simulations. The mesh size, buckling modes and stiffener profiles are noted.

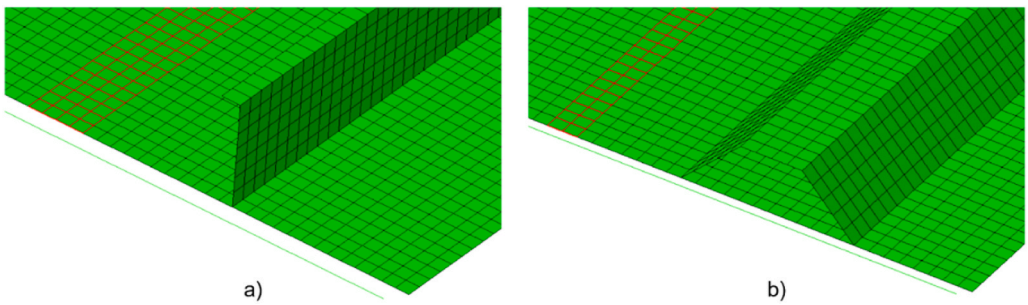

Fig. 7. Mesh of stiffened panels: a) panels with L-shaped stiffeners, b) panels with closed stiffeners. The HAZ is displayed in red.

2.6. Summary

The numerical modelling is important with respect to buckling prediction. The assumptions adopted in the simulations are summarized.

Due to the lack of measurements, it is assumed that all extruded panels that were assembled by welding possess the same geometries. In reality, differences existed (e.g., varying thickness), and this will influence the initial buckling position [22]. The deformation magnitude after welding was only provided in the middle of each stiffener and used as the amplitude in sinusoidal imperfection model. If the actual field is used the influence may be substantial. The boundary conditions for the loaded edges are modelled physically with the rigid beam model. It is still not an exact replication of the loading system in the reference experiments. While the unloaded edges are restrained by the fixture rail, this is modelled as simply supported boundaries. However, the support structures cannot be perfectly rigid in reality.

The material properties are critical in buckling simulations so it should be modelled as accurate as possible [22]. The widely used Ramberg-Osgood material model is assigned for the plate, stiffeners and HAZ where the different parameters are calibrated from the reference experiments. However, the data is limited so the whole stress-strain curve may not be entirely correct. Furthermore, any

material inhomogeneities are not included in this work. The yield stress of HAZ material is based on approximate measurements in the reference experiments. Although the value adopted is within a range that is normally assumed [5,13,23–25], uncertainties still exist.

Strain rate effects are neglected. On the one hand, the loading speed is small enough. On the other hand, the used AA6082-T6 alloys have been found to be almost rate insensitive [26,27]. It is thus considered acceptable to use static material properties in this buckling investigation.

The HAZ size is based on experimental measurements by Rønning et al. [4]. The size, 20 mm, is consistent with the suggested value by Eurocode 9 [28], but it is slightly lower than 25 mm adopted by other research [5,13,23–25]. Only residual stresses along the welding direction are assumed considering the small magnitude in other directions [29]. It is also noticed that the transverse residual stress could be increased by a higher degree of restraint during welding [30]. The residuals stress is assumed to be uniformly distributed within the HAZ. In reality it is non-uniform, but the influence was found to be minor [31].

3. Results and discussions

3.1. Simulation verification

In general, the simulations are consistent with the reference experiments. The load end-shortening curves have the same slope in the elastic range and yield a similar trend after buckling. A few examples are shown in Fig. 8; all simulation results are shown in the appendix.

The largest load from the load end-shortening curve is regarded as the ultimate load in the simulations. The percent deviation between the predicted ultimate load in the simulations and the reported ultimate load in the reference experiment (*ultimate load deviation* for short) is defined as:

$$ULD = \frac{F_{sim} - F_{\exp}}{F_{\exp}} \tag{2.3}$$

where.

ULD is the ultimate load deviation.

F_{sim} is the predicted ultimate load in the simulations,

and $F_{\exp}$ is the reported ultimate load in the reference experiments.

The ultimate load deviation is plotted as a function of the reduced slenderness ratio (*slenderness ratio* for short) of the panels, as

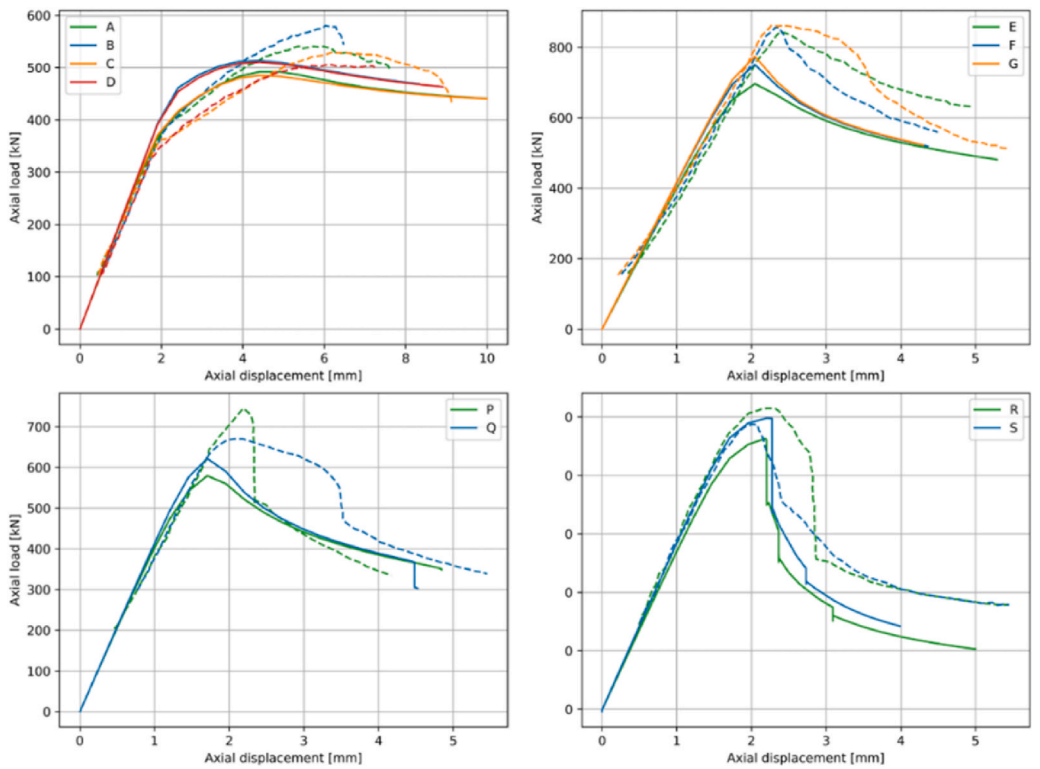

Fig. 8. Load end-shortening curves for selected panels. The experiments are plotted with dashed lines, and the simulations are plotted with solid lines. Different cases are indicated by different colors.

shown in Fig. 9. In most cases, the buckling modes from the simulations are consistent with those observed in the experiments, but they deviate in five of the 21 cases, either with an opposite buckling direction or an incorrect mode. The difference is mostly within 15%. The simulations generally produce conservative predictions of the ultimate load.

The simulations underpredict the panel strength after initial yielding in most cases. Based on the load end-shortening curves calculated in this study, the panels with free edges (Panel N to U) show less divergence with the experimental results in the post-buckling range than those of the panels with simply supported edges (Panel A to M). A possible reason is that the simply supported edges implicitly provide rigid support in vertical direction. The numerical prediction might be better if the boundary conditions are physically modelled. It is also found that the curves of the longer panels (2 m) are closer to the experimental ones than those of the shorter panels (1 m). This may be related to the different buckling modes. The flexural buckling of the longer panels is less sensitive to material properties and imperfection fields than is the stiffener tripping of the shorter panels, so it will be less influenced by the modelling uncertainties. Although the numerical simulations in this study are conducted in a similar manner as the reference experiments, it is impossible that they can be exactly the same due to lack of information, such as imperfection fields and material variations. The inconsistences may result in different failure positions and hence, different structural resistance for the same axial displacement, compared to the reference experiments. It was found that a small difference in the initial numerical setups may result in a large discrepancy with the experiments. Thus, a detailed parametric study may shed light on the importance of this when the experimental data is insufficient.

3.2. Inertia effects

Simulations are also conducted with the 'Static, Riks' solver, which does not account for inertia effects. In some cases, the simulation results in an unreasonably large ultimate load, such as Panel O, which is shown on the left of Fig. 10.

In some cases, the static solver obtains a stable solution after several unloading-loading loops. The ultimate load point from the reference experiments would be 'passed by' during this process. Thus, an ultimate load that is too large may be produced by the simulations, such as the panels shown in Fig. 11.

The ultimate load deviation as a function of the slenderness ratio obtained from simulations with the static solver is shown in Fig. 12. In general, the difference is greater than that obtained from simulations with the dynamic solver, as shown in Fig. 9. In some cases, an excessively large ultimate load is obtained, resulting in a difference of up to 50%. When the 'Static, Riks' solver is used, the correct buckling mode struggles to develop further after stiffener tripping. The panel tends to 'bounce back' towards the original configuration, causing the load end-shortening curve to reverse. Only in one of the cases shown in Fig. 12 (Panel L) the solver succeeded in finding the correct elastic spring-back path. It is concluded that the ultimate load may sometimes be difficult to calculate numerically with the 'Static, Riks' solver.

In the dynamic analysis, inertia forces 'push' the tripping stiffener into the final panel-buckling mode without any numerical issues. This is especially important for stocky panels. To further investigate this effect, simulations with a loading speed ranging from 0.5 to 32 times of that in the reference experiments are conducted. The force end-shortening curves for two cases that suffered from numerical instabilities are plotted in Fig. 13. They demonstrate that the inertia forces in the dynamic solver change the initial buckling point and ultimate load.

An increasing ultimate strength is observed for a loading speed up to four times of that in the experiments. Larger loading speeds may reduce the structural resistance instead of further enhancing it. For example, the '16×' case of Panel K shows a smaller ultimate strength than '4×' and '8×' cases. The trend reveals that the bifurcation buckling problem in this case is very sensitivity to the detailed parameters adopted. The existence of inertia forces influences the choice of failure path between several closely spaced solutions. If the magnitude of inertia force changes, the initial yielding position and final failure patterns change accordingly as shown in Fig. 14. It is

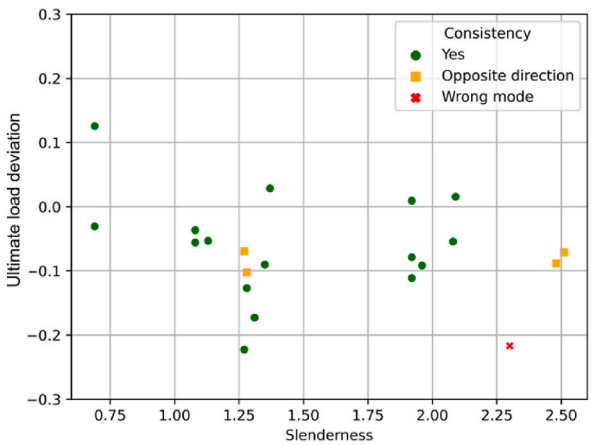

Fig. 9. Ultimate load deviation of the ultimate load between the 'Dynamic/Implicit, Quasi-static' simulations and the reference experiments. The consistency of the buckling mode is indicated by different markers and colors.

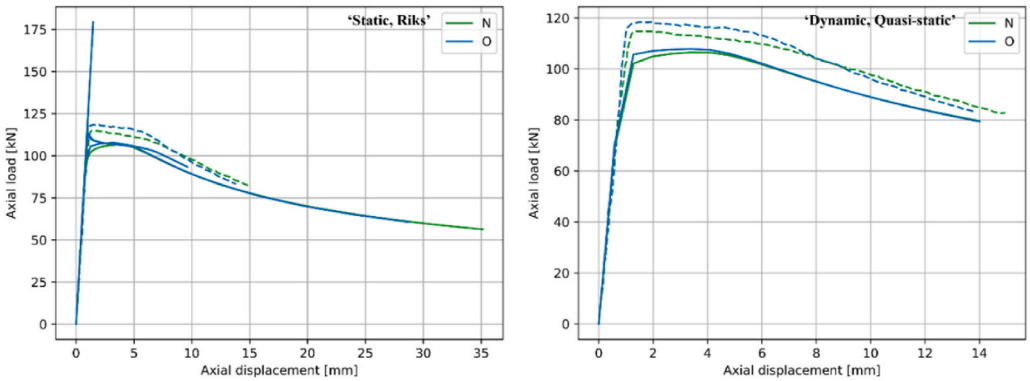

Fig. 10. Load end-shortening curves for Panels N and O with an unreasonably large ultimate loads using the 'Static, Riks' solver. The experiments are plotted with dashed lines, and the simulations are plotted with solid lines. Different cases are indicated by different colors.

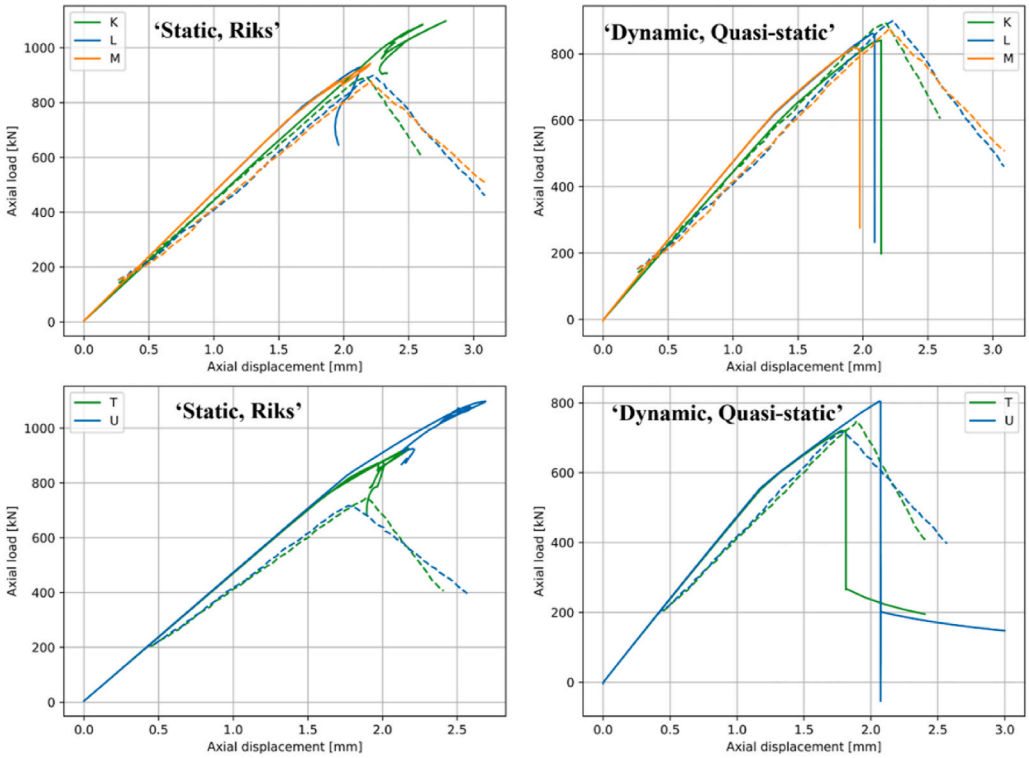

Fig. 11. Load end-shortening curves for panels with several unloading-loading loops using the 'Static, Riks' solver. The experiments are plotted with dashed lines, and the simulations are plotted with solid lines. Different cases are indicated by different colors.

noticed that the initial yielding area of '8×' and '32×' cases is similar, as is the final failure pattern. Accordingly, the load end-shortening curves of the two cases in Fig. 13 b) possess the same trend between yielding point and ultimate load point. The difference of the ultimate load may be due to inconsistent tripping direction of one stiffener, as indicated by red arrows in Fig. 14.

Although the 'Static, Riks' solver could be used to satisfactorily predict the post buckling behavior of panels, the potential unstable numerical behavior around the ultimate load should be avoided. With the 'Dynamic/Implicit, Quasi-static' solver, the artificially large ultimate load values are corrected by inertia effects. Thus, the maximum axial load can be directly regarded as the ultimate load. Notably, the ultimate load of stocky panels is better predicted with the dynamic solver. The left side of Fig. 9, with small slenderness ratios, shows that a smaller difference is obtained than in Fig. 12.

In the reference experiments, local stiffener buckling is also observed for panels with closed stiffeners. As in the case of flexural buckling, local buckling is better predicted by the 'Dynamic/Implicit, Quasi-static' solver. Panel Q is taken as an example and is shown in Fig. 15. However, this phenomenon may be neglected, as it has little effect on the ultimate load and the load end-shortening curves.

Besides introducing inertia forces to stabilize the solution with the dynamic solver, it was found that the change of loading scenarios

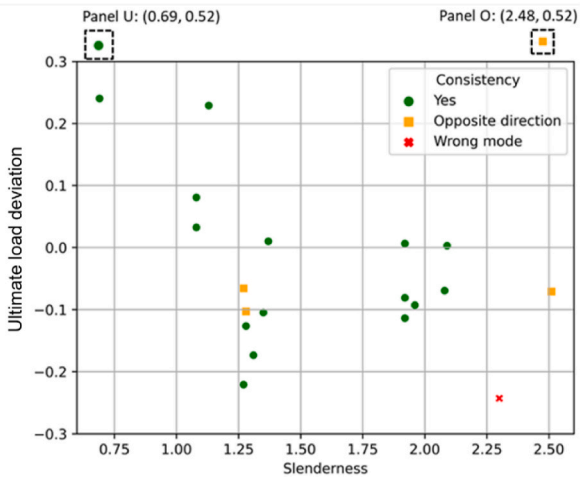

Fig. 12. Ultimate load deviation of the ultimate load obtained from 'Static, Riks' simulations and reference experiments. The consistency of the buckling mode is indicated by different markers.

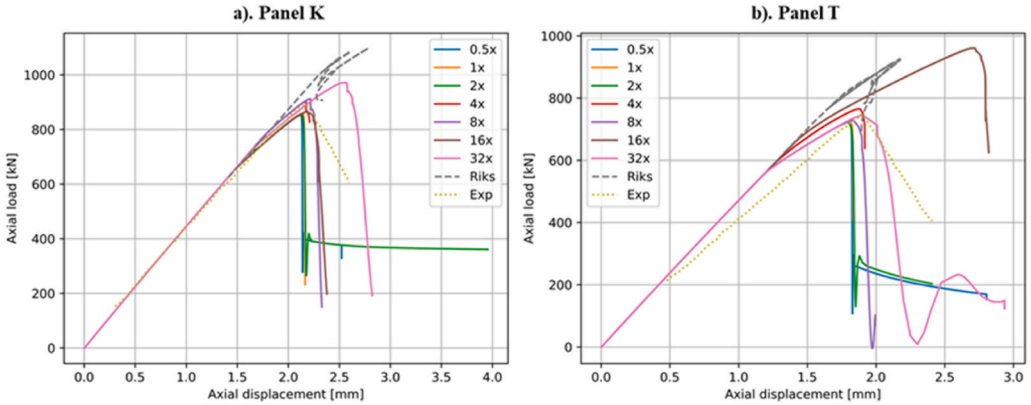

Fig. 13. Load end-shortening curves with different loading speeds. The multiple of loading speed with 'Dynamic/Implicit, Quasi-static' solver is noted. 'Riks' and 'Exp' indicates the 'Static, Riks' solver and experiment, respectively.

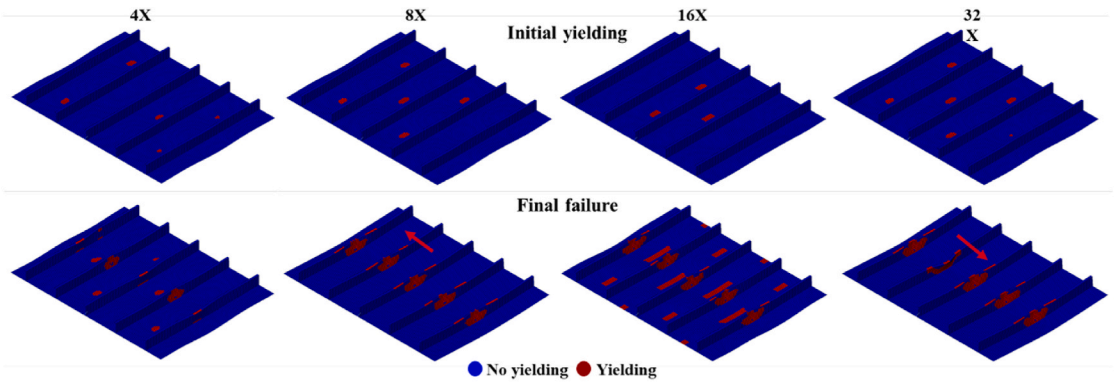

Fig. 14. Initial yielding and final failure patterns of Panel T. The multiple of loading speed with 'Dynamic/Implicit, Quasi-static' solver is noted.

reduced the numerical instabilities in some cases. By using force instead of displacement to introduce the compression, the numerical insatiability of Panel K is found eliminated, but the issue still exists for Panel T, as shown in Fig. 16. It is also possible that the instability problem may be mitigated by introducing an additional imperfection in the form of a scaled buckling mode from a bifurcation point

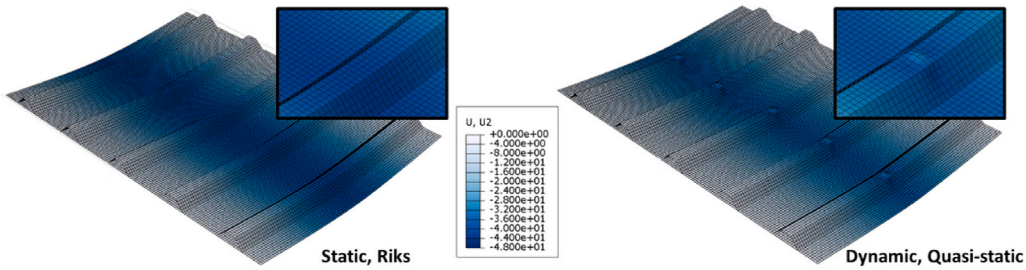

Fig. 15. Final configuration of Panel Q in simulations with different solvers. 'U2' indicates the vertical deformation. The local stiffener buckling is predicted by the 'Dynamic/Implicit, Quasi-static' solver, as shown in zoomed view.

analysis close to the expected peak load.

Static solvers are widely used in numerical simulations of panel buckling. However, the results obtained by the dynamic solver indicates that stiffener tripping for stocky panels with L-shaped stiffeners is largely related to inertia forces. If inertia forces are not considered, numerical instability may yield inaccurate ultimate load predictions. Thus, the load-displacement curves should be checked carefully in the case of stocky panels. The maximum axial load recorded in the simulations may not accurately reflect the ultimate load, and the results could be overestimated. To obtain a more reliable prediction of the ultimate load, the dynamic solver is suggested for stocky panels. The inclusion of inertia effects improves numerical stability bringing the simulation closer to reality.

3.3. Sensitivity analysis of welding effects

To identify the trend of results, the strength reduction due to the welding effects (*strength reduction* for short) is defined as:

$$SR = \frac{F_{noHAZ} - F_{\mathrm{HAZ}}}{F_{noHAZ}} \tag{2.4}$$

where.

SR is the strength reduction.

F_{noHAZ} is the predicted ultimate load in the simulations without HAZ effects,

and F_{HAZ} is the predicted ultimate load in the simulations with HAZ effects.

It should be noted that a negative strength reduction value means that the ultimate strength is increased by the introduced HAZ effects.

3.3.1. Residual stress magnitude

A literature search reveals that the scale of the tensile residual stress ranges from 75% to 100% of the HAZ material yield stress and that the compressive residual stress is balanced [5,9,10,32]. Some researchers also have neglected the residual stress [11,19,32]. A parametric study is conducted to investigate the influence of varying residual stress levels.

The ultimate load deviation and strength reduction is shown in Fig. 17. Only one case is shown in the figure if several panels have the same slenderness ratio. Erroneous predictions of buckling modes do occur in the simulations. Such cases are circled and excluded from discussion. The least squares regression lines of the strength reduction are plotted for different HAZ assumptions and boundary conditions. The assigned HAZ width is as illustrated in Section 2.3. The sensitivity of the ultimate load deviation to the residual stress levels is moderate, so the assumed 70% level in this study should be acceptable. Panels with L-shaped stiffeners (square markers) are more sensitive to residual stress than panels with closed stiffeners (circle markers). This is mainly because the HAZ width of the panels with L-shaped stiffeners is assumed to be larger due to the different welding methods.

Based on the strength reduction, the simulations generally show two opposing trends for increasing tensile residual stress: the ultimate load increases for stocky panels, while it decreases for slender panels. For panels with a slenderness ratio less than 2, the simulations show that the ultimate load generally increases with increasing tensile residual stress. However, the ultimate load decreases slightly when the tensile residual stress increases from 0% to 40% for very stocky panels (slenderness ratios of 0.69 and 1.08). The increase in the ultimate load with increasing residual stress is also observed in simulations by Li et al. [14], with a similar geometry and a slenderness ratio of approximately 1.1. For panels with a slenderness ratio larger than 2, this work shows that the ultimate load decreases with increasing tensile residual stress. On the average, the strength reduction of the simply supported panels (solid curves) is higher than that of the free panels (dotted curves). The slope of the former is also larger. The restrained edges make the panels more sensitive to the introduction of residual stresses when the panel is very stocky or very slender.

The simulations with and without residual stress are compared in Fig. 18. The tensile residual stress discussed here is assumed to be 70% of the HAZ material yield stress, which is the same level as the results plotted with yellow dots in Fig. 17.

Generally, the change in ultimate load is not large, regardless of whether it increases (stocky panels) or decreases (slender panels). However, the magnitude of the increase is slightly larger than the magnitude of the decrease. This is because of the slenderness dependence of the HAZ effects, which will be discussed later.

The introduction of residual stress may correct the inconsistency of the buckling mode prediction in some cases, as indicated by

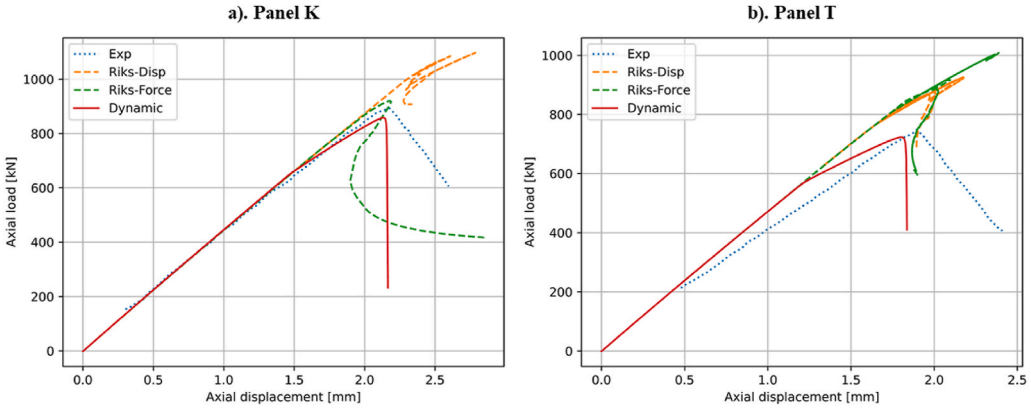

Fig. 16. Load end-shortening curves with different loading methods. The 'Disp' and 'Force' indicates the displacement-controlled and force-controlled buckling simulations, respectively.

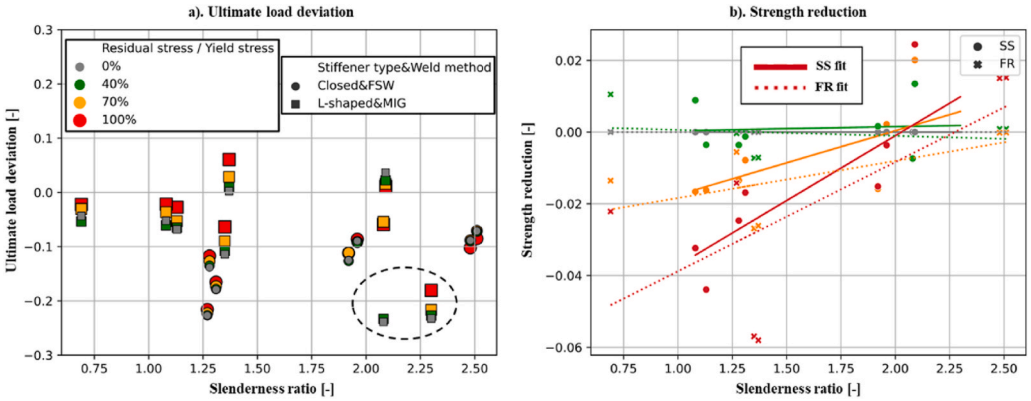

Fig. 17. Numerical results with varying residual stress levels. The percentage of the residual stress levels is indicated by different colors. The stiffener types and welding methods are indicated by different markers. 'SS' indicates simply supported boundaries. 'FR' indicates free boundaries.

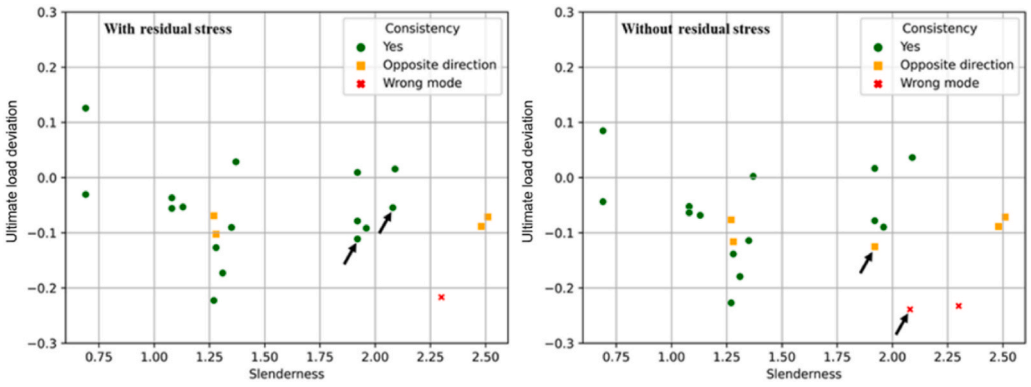

Fig. 18. Ultimate load deviation with or without the residual stress. The consistency of the buckling mode is indicated by different markers. Cases with buckling mode correction are noted with black arrows.

black arrows in Fig. 18. This reflects the fact that the existence of residual stress is more realistic. However, given that the introduced residual stress may strengthen the panels, the modeling of the residual stress in the numerical simulations should be carefully evaluated. A very high residual stress level, even levels equal to the HAZ material yield stress, should be avoided, as this may overestimate the ultimate load, as shown by the red dots in Fig. 17.

3.3.2. HAZ width

In this work, the HAZ width is assumed based on the measurements of Rønning et al. [4], with 10 mm and 20 mm widths assigned on each side for FSW and MIG welded panels, respectively. To verify this assumption, the influence of the HAZ width is analyzed by varying the width from 10 to 40 mm.

The ultimate load deviation and strength reduction excluding residual stresses are shown in Fig. 19. As before, circled cases with incorrect buckling mode predictions are not discussed.

There is a weak trend of decreasing ultimate strength with a larger HAZ width. The reduction is small; the maximum value is approximately 0.3%. The limited influence of HAZ width on ultimate strength with only material softening and no residual stresses taken into account has also been observed by other researchers. Chen [33] compared the strength reduction after increasing the HAZ width without residual stress. In his simulations, the HAZ material was 40% softened from the base material, which is the same as in this work. For a panel with a slenderness of 0.651, he found that the strength reduction changed from 0.71% for 5 mm to 4.25% for 40 mm. The decrease was not large. Li et al. [14] used the same geometry and material as Panel K to investigate the influence of the HAZ width. The ultimate load changed by approximately 0.4% as the HAZ increased from 0 to 90 mm in that study. Thus, it is concluded that the HAZ width has a minor effect on the ultimate load when residual stress is not included.

When residual stress is included, the ultimate load deviation and strength reduction are larger as shown in Fig. 20. For the panels with closed stiffeners, the mean ultimate load deviation is minimum with an HAZ width of 10 mm, reveling that the assumed HAZ width is reasonable. Although the average ultimate load deviation can be reduced slightly (1.8%) with a larger HAZ width, the ultimate strength prediction in some cases will be too unconservative. The influence of residual stresses is proved to be more critical than the material softening in the studies cases, together with the strength reduction in Fig. 19. As for the effects of the boundary conditions, the similar trend as that of increasing residual stress magnitude is observed.

3.4. Slenderness dependence of welding effects

The sensitivity of the ultimate load with respect to the HAZ width depends on the slenderness ratio. Fig. 21 shows the absolute strength reduction after increasing the HAZ width from 0 mm to 40 mm on each side. The ultimate load of the stocky panels is particularly sensitive to changes in the HAZ width, whether excluding or including residual stresses.

It is found that the panel with large slenderness ratios are less influenced by the introduction of the material softening and residual stresses. The reason could be that the materials do not reach high stress levels in this case. The material yielding and stress distribution of two panels at the initial buckling point are shown in Fig. 22. The slenderness ratio of chosen Panel N and Panel T is the largest and smallest in the simulations, respectively. The HAZ effects are not considered in a) and b). Within the area between two stiffeners, where the HAZ is assumed, the stresses are higher for Panel T than Panel N. Thus, the Panel N will be less influenced by the material property change from HAZ effects as shown in c). For the Panel T, the yielding area and the stress distribution change obviously as shown in d), thus the ultimate load changes. This trend is similar to the absolute strength reduction for increasing HAZ width shown in Fig. 21. The ultimate load changes more for panels with small slenderness ratios than for those with large slenderness ratios, even when the change in the HAZ width is the same.

The slenderness dependence of the residual stress effect is also observed in this study. The strength reduction with the HAZ width of 20 mm on each size including residual stresses is shown in Fig. 23. Although the tensile residual stress in the parametric investigation by Chen [33] was assumed to be 75% of the HAZ material yield stress instead of 70% in this work, it is comparable considering the 5% difference is small. This study shows that when residual stress is included, the ultimate load decreases or increases depending on the slenderness ratio. For slender panels, the ultimate load decreases. For stocky panels, the ultimate load increases. The slenderness ratio where the transition occurs is approximate 2 and 2.25 for panels with open and closed stiffeners, respectively.

Similarly, the combined effect of the softened material and the residual stress may decrease or increase the panel strength, as

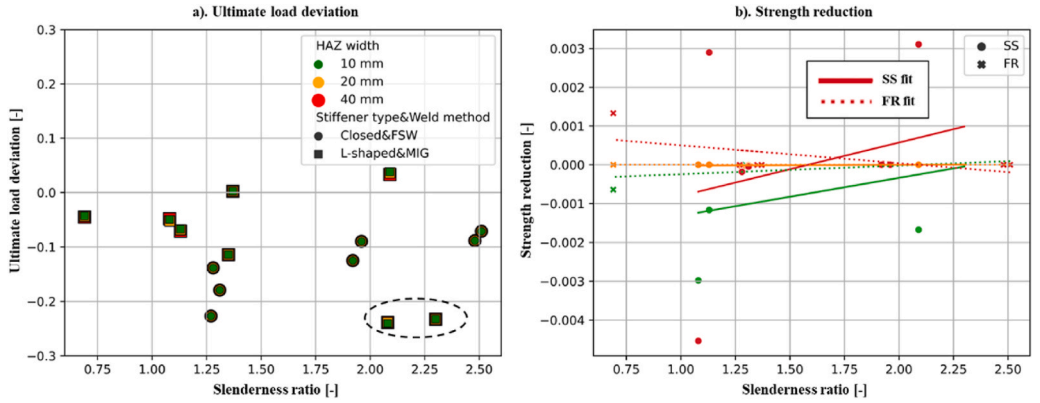

Fig. 19. Numerical results with varying HAZ width excluding residual stresses. The width of the HAZ is indicated by different colors. The stiffener types and welding methods are indicated by different markers. 'SS' indicates simply supported boundaries. 'FR' indicates free boundaries.

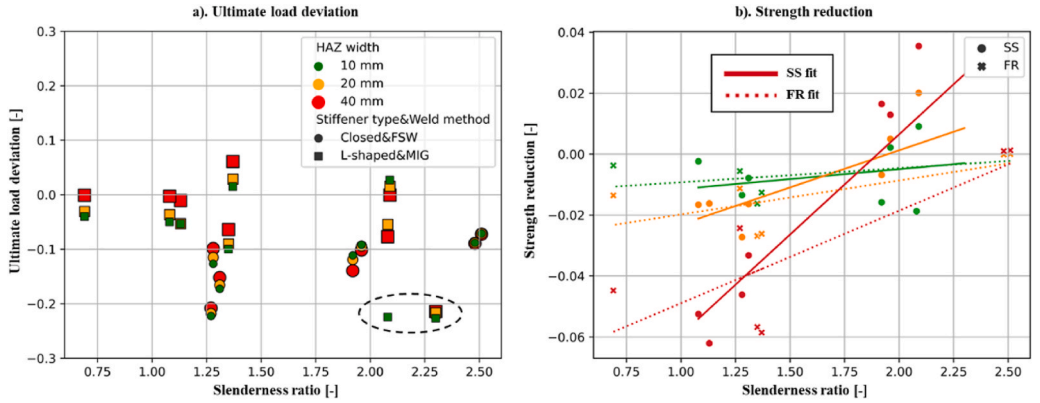

Fig. 20. Numerical results with varying HAZ width including residual stresses. The width of the HAZ is indicated by different colors. The stiffener types and welding methods are indicated by different markers. 'SS' indicates simply supported boundaries. 'FR' indicates free boundaries.

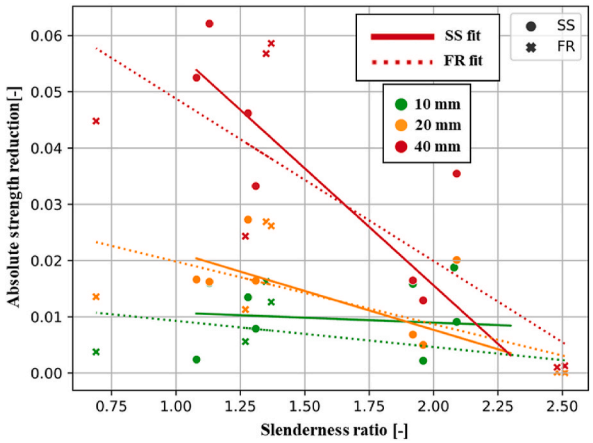

Fig. 21. Absolute strength reduction after increasing the HAZ width from 0 mm to 40 mm on each side.

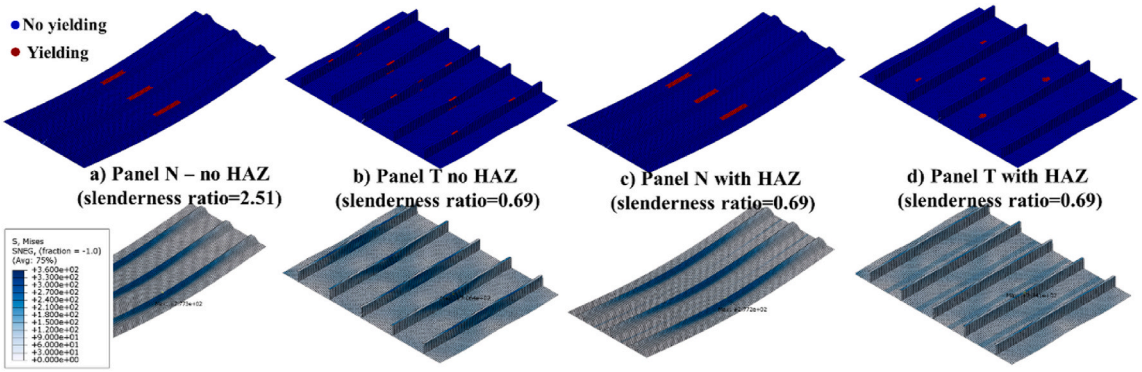

Fig. 22. Material yielding and Von Mises stresses of the panel N and T at the initial buckling point.

indicated by the gray dots (Chen's work) in Fig. 23. For panels with closed stiffeners, the slenderness ratio of strengthened cases was found mainly between 0.5 and 2. When the slenderness ratio is larger than 2, the strength is likely to be decreased. According to our findings, the transition slenderness ratio is around 2.25 for the same stiffener shape. Thus, the two works are generally consistent. A similar slenderness range dependence was also observed for panels with L-shaped stiffeners in this work and panels with T-type stiffeners in Chen's work. The conducted simulations supplement the cases in which the ultimate strength is increased by welding effects.

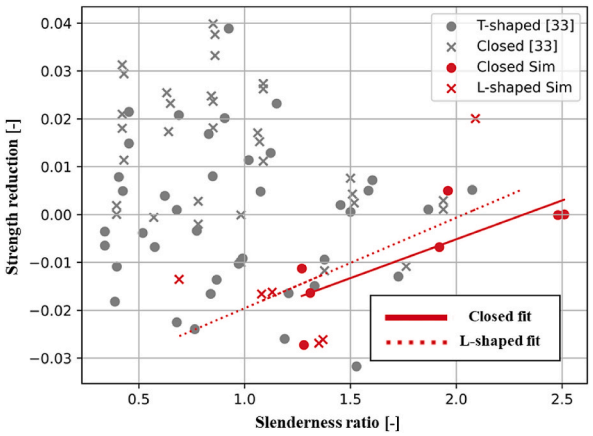

Fig. 23. Strength reduction comparison with approximate HAZ effects assumptions. The results from the simulations are plotted in red. The results from the work by Chen [33] are plotted in gray.

In this work, two slenderness dependencies are observed:

First, the ultimate load of stocky panels is more sensitive to HAZ effects. This dependence is found to be related to the stress distributions, which are larger for the smaller slenderness ratios. Thus, the initial buckling position and the failure mode are more influenced. Observing that stocky panels experience mainly stiffener tripping mode while the slender panels show mainly flexural buckling mode in the simulations, the dependence is also believed to be related to the different buckling modes. The physics underlying such a dependence should be investigated further in details.

Second, the addition of residual stress may increase or decrease the ultimate load, depending on the slenderness ratio. Within a certain range, the ultimate load is likely to increase due to the presence of tensile residual stress. Outside of this range, the compressive residual stress dominates, reducing the ultimate load. The range of the slenderness ratio depends on the stiffener type.

It is also observed that the ultimate load may increase or decrease due to residual stress even for the same slenderness ratios. The dependence of the strength change on other parameters, such as the plate slenderness ratio and the web slenderness ratio, should be investigated with more simulation cases. Multifactor influencing mechanics may be revealed.

4. Conclusions

The nonlinear finite element method was used to simulate the buckling of aluminum extruded panels. The numerical simulations were verified by comparison with experiments by Aalberg et al. [3]. Welding-induced geometrical and mechanical imperfections were assigned carefully. The buckling modes, load end-shortening curves, and ultimate loads were consistent with the results of the reference experiments. The effects of inertia in buckling were investigated by analyzing with the static and dynamic solvers. The sensitivity of the ultimate load with respect to the welding effects was determined by parametric studies. The main conclusions are summarized as follows:

- The static solver is commonly used in buckling simulations, but the inertia forces that are neglected in this solver are found to be important in pushing the buckling process forward. When the stiffener-tripping mode occurs, the inertia forces are found to play a particularly important role. Thus, the dynamic solver is suggested for simulations of this case, which generally occurs for stocky panels with open stiffeners. The inclusion of inertia effects improves numerical stability, thus avoiding severe overprediction of the ultimate load.
- The residual stress model should be checked carefully. Inconsistencies in the predicted buckling mode are sometimes corrected when residual stress is considered. However, including the residual stress may strengthen the panels, resulting in overestimations of ultimate load. Large residual stress levels, such as those equal to the HAZ material yield stress, should therefore be avoided.
- The influence of welding on the ultimate load is highly dependent on the slenderness ratio. The ultimate load of stocky panels with low slenderness ratios is more sensitive to the heat-affected zone. It is believed that this is related to the stress distribution, triggering different buckling modes. The physics behind this should be investigated further. The residual stress increases the ultimate load within a certain range of the slenderness ratio, while it decreases the ultimate load outside this range. The range of the slenderness ratio depends on the stiffener type.

Declaration of competing interest

The authors declare that they have no known competing financial interests or personal relationships that could have appeared to influence the work reported in this paper.

Acknowledgments

The authors gratefully acknowledge the support from the Research Council of Norway under the Knowledge-Building Project for Industry Robot Welding of Aluminum Ship Hulls [grant number: KPN295138]. Part of this work is also supported by the Centre for Autonomous Marine Operations and Systems (AMOS) [project number: 223254]. We are grateful to A. Aalberg, M. Langseth and P. K. Larsen for allowing reproductions of their excellent research work.

Appendix A. Geometries of the stiffened panels

Table A1
Dimensions of the stiffened panels in the simulations. The table is reproduced from Table 1 of the work by Aalberg et al. [3].

Panel	Stiffener section	a [mm]	b [mm]	Cross-section [mm]					Imperfections [mm]									
				t_1	t_2	t_3	s_2	h	$w_{0,1}$	$w_{0,2}$	$w_{0,3}$	$w_{0,4}$	$w_{0,5}$	$v_{0,1}$	$v_{0,2}$	$v_{0,3}$	$v_{0,4}$	$v_{0,5}$
Support along longitudinal edges																		
A	closed	2000	1400	3.04	3.02	3.06	42	40.8	0.4	0.0	0.3	0.8	0.5					
B	closed	2000	1400	3.10	3.08	3.04	42	41.1	1.9	1.4	2.9	2.4	0.2					
C	closed	2000	1400	3.10	3.08	3.04	42	41.1	−2.6	0.4	1.9	0.3	−2.2					
D	closed	2000	1400	3.10	3.08	3.04	42	41.1	1.5	2.1	3.2	2.1	1.5					
E	closed	1020	1400	3.10	3.06	3.02	42	41.1	0.0	0.1	0.2	0.0	0.0					
F	closed	995	1400	3.10	3.06	3.04	42	41.1	0.5	0.9	1.0	1.0	0.0					
G	closed	995	1400	3.10	3.06	3.04	42	41.1	0.5	1.5	1.2	1.4	0.5					
H	open	2000	1262.5	4.95	2.96	4.36	14.8	76.1	0.5	1.0	2.0	0.5	0.0	0.0	1.0	−1.0	1.5	−1.0
I	open	1985	1262.5	4.94	2.95	4.35	14.9	76.2	2.0	2.6	2.5	2.0	2.2	−0.5	−0.4	−0.1	−0.1	1.5
J	open	2000	1262.5	4.87	2.97	4.37	14.9	76.5	2.5	3.0	3.5	3.0	2.0	0.3	−0.3	−1.3	0.0	0.8
K	open	1023	1262.5	4.87	2.97	4.37	14.9	76.5	0.3	1.3	1.5	1.4	0.6	0.0	0.1	0.0	0.0	0.0
L	open	957	1262.5	4.85	2.95	4.35	14.8	76.2	0.5	1.2	1.5	1.2	0.5	1.0	−0.5	−0.5	0.0	−1.5
M	open	957	1262.5	4.85	2.95	4.35	14.8	76.2	0.2	0.4	0.5	0.1	0.1	0.0	0.0	0.3	−1.5	−1.0
No support along longitudinal edges																		
N	closed	2004	730	3.00	3.06	3.01	42	41.1		0.4	0.6	0.8						
O	closed	2000	840	3.04	3.02	3.06	42	40.8		1.2	1.8	1.8						
P	closed	998	1400	3.10	3.06	3.04	42	41.1	0.1	0.2	0.2	0.2	0.1					
Q	closed	998	1400	3.10	3.06	3.04	42	41.1	0.2	1.5	1.3	1.3	0.8					
R	open	1985	757.5	4.94	2.95	4.35	14.9	76.2		0.2	1.5	1.5			1.0	−0.5	1.0	
S	open	1985	757.5	5.10	3.05	4.42	15	76.6		2.3	1.0	1.0			1.4	0.6	0.2	
T	open	957	1262.5	4.85	2.95	4.35	14.8	76.2	0.3	0.3	0.4	0.4	0.3	−0.8	−0.2	0.2	0.0	0.0
U	open	957	1262.5	4.85	2.95	4.35	14.8	76.2	1.2	1.5	1.2	1.2	1.5	0.8	−0.2	0.3	0.3	1.0

Appendix B. Load end-shortening curves of simulations

The reference experiments and simulations are plotted with dashed lines and solid lines, respectively.

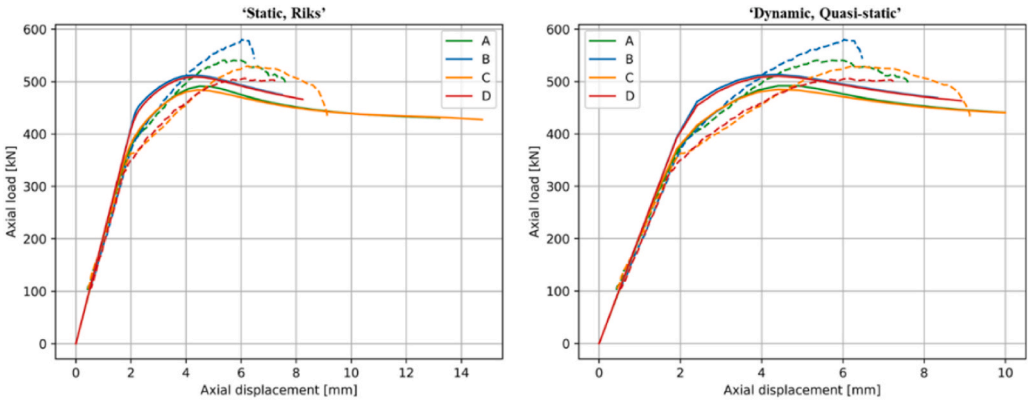

Fig. B1. Load end-shortening curves for Panel A, B, C and D. .

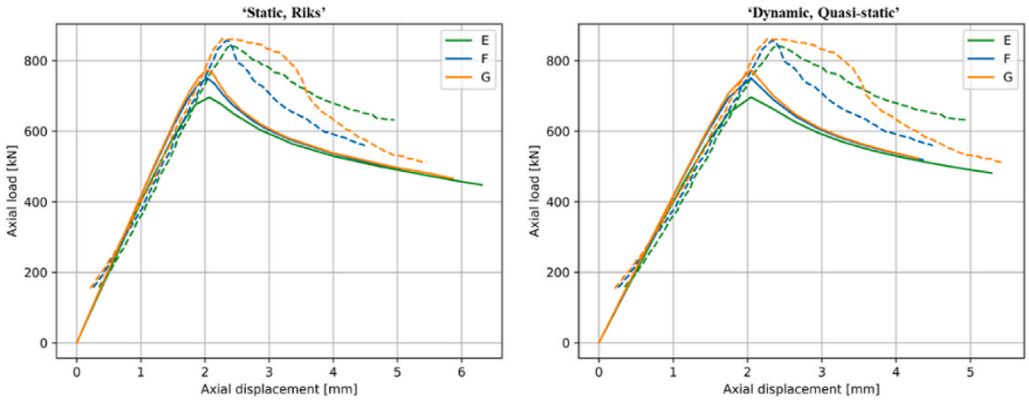

Fig. B2. Load end-shortening curves for Panel E, F and G.

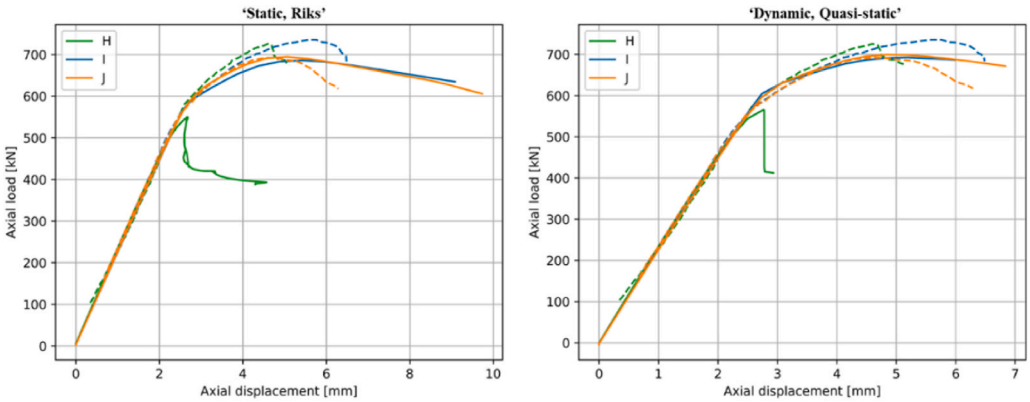

Fig. B3. Load end-shortening curves for Panel H, I and J.

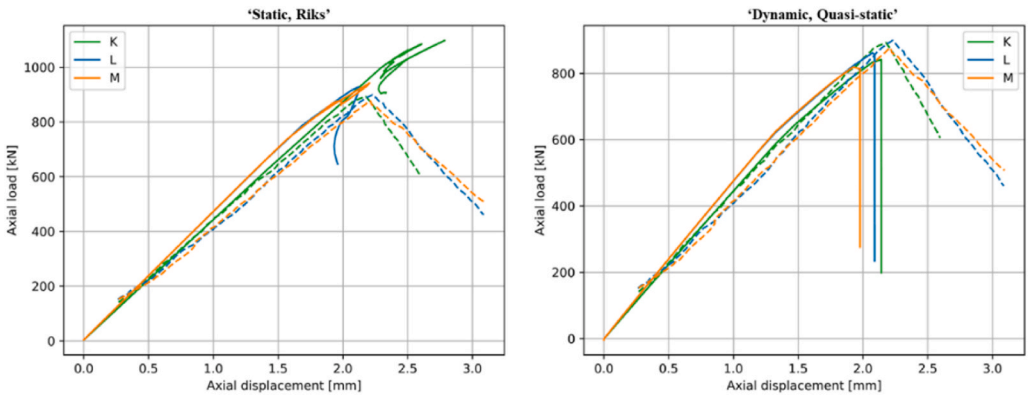

Fig. B4. Load end-shortening curves for Panel K, L and M.

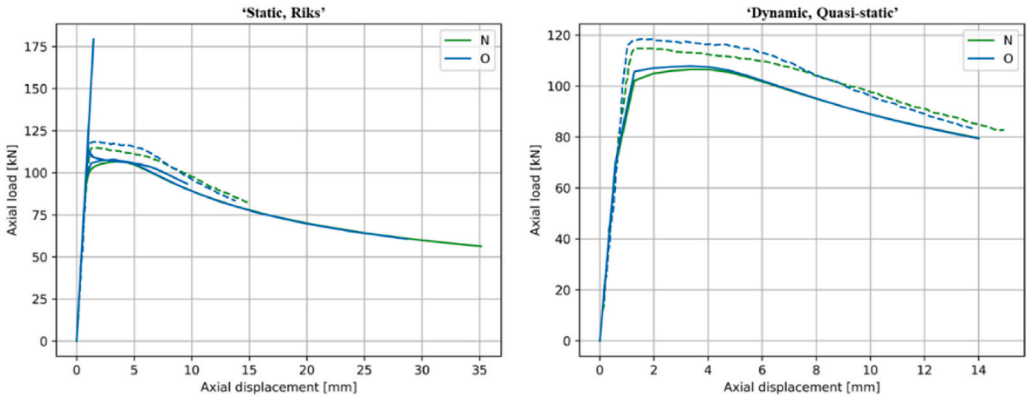

Fig. B5. Load end-shortening curves for Panel N and O.

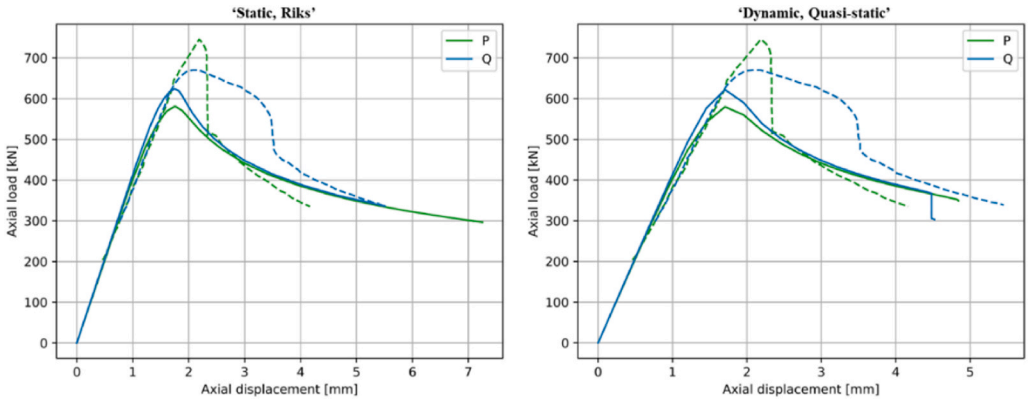

Fig. B6. Load end-shortening curves for Panel P and Q.

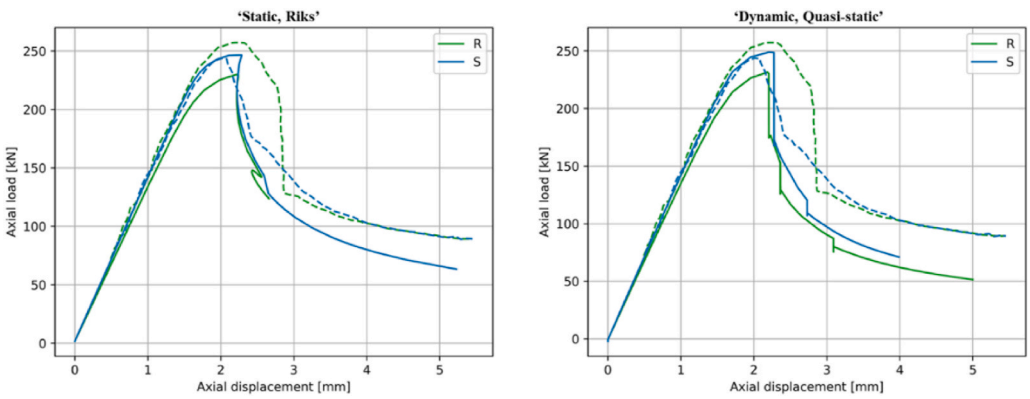

Fig. B7. Load end-shortening curves for Panel R and S.

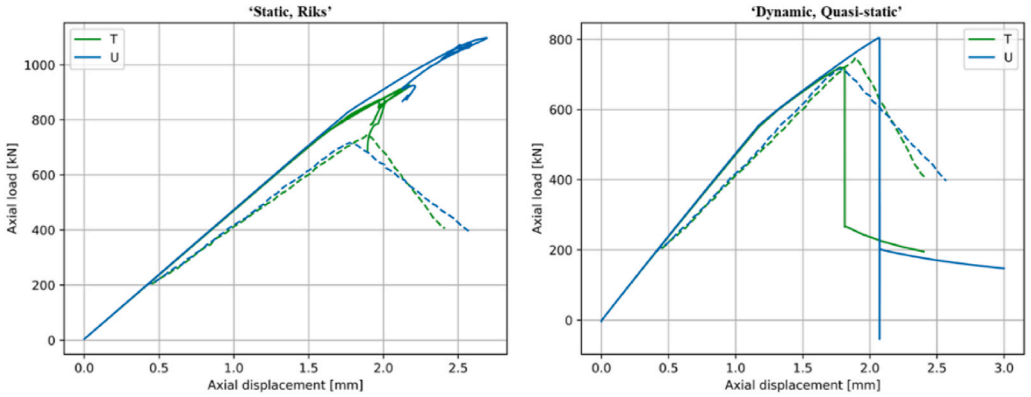

Fig. B8. Load end-shortening curves for Panel T and U.

References

[1] Stenius I, Rosén A, Kuttenkeuler J. On structural design of energy efficient small high-speed craft. Mar Struct 2011;24(1):43–59. https://doi.org/10.1016/j.marstruc.2011.01.001. 2011/01/01.

[2] Lundberg S. Use of aluminium structures in the offshore Industry. Key Eng Mater 2016;710:22–31. https://doi.org/10.4028/www.scientific.net/KEM.710.22.

[3] Aalberg A, Langseth M, Larsen PK. Stiffened aluminium panels subjected to axial compression. Thin-Walled Struct 2001;39(10):861–85. https://doi.org/10.1016/S0263-8231(01)00021-0. 2001/10/01.

[4] Rønning L, Aalberg A, Kristian Larsen P. An experimental study of ultimate compressive strength of transversely stiffened aluminium panels. Thin-Walled Struct 2010;48(6):357–72. https://doi.org/10.1016/j.tws.2010.01.015.

[5] Zha Y, Moan T. Experimental and numerical prediction of collapse of flatbar stiffeners in aluminum panels. J Struct Eng 2003;129(2):160–8.

[6] Zha Y, Moan T, Hanken E. Experimental and numerical study of torsional buckling of stiffeners in aluminium panels. In: The tenth international offshore and polar engineering conference. International Society of Offshore and Polar Engineers; 2000.

[7] Paik JK. "Buckling collapse testing of friction stir welded aluminum stiffened plate structures," Report SR-1454. Washington (DC): Ship Structure Committee; 2009.

[8] Paik JK, Andrieu C, Cojeen HP. Mechanical collapse testing on aluminum stiffened plate structures for marine applications. Mar Technol SNAME News 2008;45(4):228–40.

[9] Rigo P, et al. Sensitivity analysis on ultimate strength of aluminium stiffened panels. Mar Struct 2003;16(6):437–68. https://doi.org/10.1016/j.marstruc.2003.09.002. 2003/08/01.

[10] Khedmati MR, Zareei MR, Rigo P. Sensitivity analysis on the elastic buckling and ultimate strength of continuous stiffened aluminium plates under combined in-plane compression and lateral pressure. Thin-Walled Struct 2009;47(11):1232–45. https://doi.org/10.1016/j.tws.2009.04.010.

[11] Khedmati MR, Bayatfar A, Rigo P. Post-buckling behaviour and strength of multi-stiffened aluminium panels under combined axial compression and lateral pressure. Mar Struct 2010;23(1):39–66. https://doi.org/10.1016/j.marstruc.2009.10.003.

[12] Paulo RMF, Teixeira-Dias F, Valente RAF. Numerical simulation of aluminium stiffened panels subjected to axial compression: sensitivity analyses to initial geometrical imperfections and material properties. Thin-Walled Struct 2013;62:65–74. https://doi.org/10.1016/j.tws.2012.07.024.

[13] Chen Q, Moan T. Material softening effect on ultimate strength of stiffened aluminium panels. In: In international conference on offshore mechanics and Arctic engineering, vol. 49101; 2010. p. 677–87.

[14] Li C, Ren H, Zhu Z, Guedes Soares C. Numerical investigation on the ultimate strength of aluminium integrally stiffened panels subjected to uniaxial compressive load. Thin-Walled Struct 2018;127(December):221–34. https://doi.org/10.1016/j.tws.2018.01.003. 2017.

[15] Farajkhah V, Liu Y. Effect of metal inert gas welding on the behaviour and strength of aluminum stiffened plates. Mar Struct 2016;50:95–110. https://doi.org/10.1016/j.marstruc.2016.07.005.

[16] Liu B, Doan VT, Garbatov Y, Wu W, Guedes Soares C. Study on ultimate compressive strength of aluminium-alloy plates and stiffened panels. J Mar Sci Appl 2020. https://doi.org/10.1007/s11804-020-00170-2.

[17] Li C, Ren H, Zhu Z, Feng G, Fu P, Guedes Soares C. Influence of model extension and boundary conditions on the buckling behaviour of aluminium integrally stiffened panels under uniaxial compressive loading. Ocean Eng 2020;216:108066. https://doi.org/10.1016/j.oceaneng.2020.108066. 2020/11/15.

[18] Khedmati MR, Zareei MR, Rigo P. Empirical formulations for estimation of ultimate strength of continuous stiffened aluminium plates under combined in-plane compression and lateral pressure. Thin-Walled Struct 2010;48(3):274–89. https://doi.org/10.1016/j.tws.2009.10.001.

[19] Khedmati MR, Memarian HR, Fadavie M, Zareei MR. Empirical formulations for estimation of ultimate strength of continuous aluminium stiffened plates under combined transverse compression and lateral pressure. Ships Offshore Struct 2016;11(3):258–77.

[20] Paik JK, Duran A. Ultimate strength of aluminum plates and stiffened panels for marine applications. Mar Technol SNAME News 2004;41(3):108–21.

[21] Hosseinabadi OF, Khedmati MR. A review on ultimate strength of aluminium structural elements and systems for marine applications. Ocean Eng 2021;232:109153. https://doi.org/10.1016/j.oceaneng.2021.109153. 2021/07/15.

[22] Ringsberg JW, et al. The ISSC 2022 committee III.1-Ultimate strength benchmark study on the ultimate limit state analysis of a stiffened plate structure subjected to uniaxial compressive loads. Mar Struct 2021;79:103026. https://doi.org/10.1016/j.marstruc.2021.103026. 2021/09/01.

[23] Kristensen Q, Moan T. Ultimate strength of aluminium plates under biaxial loading. In: Proceedings of the fifth international conference on fast sea transportation. New York; 1999.

[24] Paik JK, van der Veen S, Duran A, Collette M. Ultimate compressive strength design methods of aluminum welded stiffened panel structures for aerospace, marine and land-based applications: a benchmark study. Thin-Walled Struct 2005;43(10):1550–66.

[25] Magoga T, Flockhart C. Effect of weld-induced imperfections on the ultimate strength of an aluminium patrol boat determined by the ISFEM rapid assessment method. Ships Offshore Struct 2014;9(2):218–35.

[26] Morin D, Kaarstad BL, Skajaa B, Hopperstad OS, Langseth M. Testing and modelling of stiffened aluminium panels subjected to quasi-static and low-velocity impact loading. Int J Impact Eng 2017;110:97–111. https://doi.org/10.1016/j.ijimpeng.2017.03.002.

[27] Chen Y, Clausen AH, Hopperstad OS, Langseth M. Stress–strain behaviour of aluminium alloys at a wide range of strain rates. Int J Solid Struct 2009;46(21):3825–35. https://doi.org/10.1016/j.ijsolstr.2009.07.013. 2009/10/15.

[28] Standard B. Eurocode 9—design of aluminium structures—. 2007.

[29] Ahn J, et al. FEM prediction of welding residual stresses in fibre laser-welded AA 2024-T3 and comparison with experimental measurement. Int J Adv Manuf Technol 2018;95(9):4243–63. https://doi.org/10.1007/s00170-017-1548-7. 2018/04/01.
[30] Ghafouri M, Ahola A, Ahn J, Björk T. Welding-induced stresses and distortion in high-strength steel T-joints: numerical and experimental study. J Constr Steel Res 2022;189:107088. https://doi.org/10.1016/j.jcsr.2021.107088. 2022/02/01.
[31] Mohammadi M, Khedmati MR, Bahmyari E. Elastic local buckling strength analysis of stiffened aluminium plates with an emphasis on the initial deflections and welding residual stresses. Ships Offshore Struct 2019;14(2):125–40. https://doi.org/10.1080/17445302.2018.1482061. 2019/02/17.
[32] Khedmati MR, Pedram M, Rigo P. The effects of geometrical imperfections on the ultimate strength of aluminium stiffened plates subject to combined uniaxial compression and lateral pressure. Ships Offshore Struct 2014;9(1):88–109. https://doi.org/10.1080/17445302.2012.726761.
[33] Chen Q. Ultimate strength of aluminium panels, considering HAZ effects. Trondheim: Norwegian University of Science and Technology, Faculty of Engineering Science and Technology, Department of Marine Technology; 2011. p. 326. 2011.